

Maximizing Sum-Rate in Holographic Active RIS-aided Uplink Near-Field Communications

Sandeep Singh[†], Keshav Singh[†], Sandeep Kumar Singh[‡], Hyundong Shin^{*}, and Trung Q. Duong[§]

[†]Institute of Communications Engineering, National Sun Yat-sen University, Kaohsiung 80424, Taiwan

[‡]Department of ECE, Motilal Nehru National Institute of Technology Allahabad 211004, India

^{*}Dept. of Electronics and Information Convergence Engineering, Kyung Hee University, Republic of Korea

[§]Faculty of Engineering and Applied Science, Memorial University, NL A1C 5S7, Canada

E-mail: m113620004@student.nsysu.edu.tw, keshav.singh@mail.nsysu.edu.tw, sksingh@mnnit.ac.in, hshin@khu.ac.kr, tduong@mun.ca

Abstract—This work proposes the integration of the holographic active reconfigurable intelligent surface (HARIS) into a multi-user uplink near-field-driven wireless communication system. In order to provide efficient resource utilization, a sum-rate maximization problem is formulated, where the equalizer design, the power allocation at each user, and the HARIS phase profile are jointly optimized under the strict constraint of QoS requirement and limited power budget at each user and HARIS. In order to tackle the non-convex nature of the formulated problem, we propose an alternating optimization (AO)-based algorithm that adopts an iterative approach and uses optimization techniques such as minimum mean square error (MMSE), convex upper bound approximation, and semidefinite relaxation (SDR) to simultaneously optimize the equalizer at the BS, beamforming at the HARIS, and power allocation at each user. Then, extensive simulations are performed to validate the efficacy and convergence of the proposed algorithm. Furthermore, we also demonstrate the impact of key system parameters, such as HARIS elements, minimum quality of service (QoS) constraint corresponding to each user, maximum receive power at the base station (BS), and maximum amplification factor.

Index Terms—Holographic active reconfigurable intelligent surface (HARIS), sum-rate maximization, power allocation, near-field, uplink.

I. INTRODUCTION

NEXT-generation wireless networks are envisioned to provide high-speed data transmission to cope with the ever-increasing consumer demands. Consequently, the power demand also increases, which has a detrimental effect on the environment [1]. This has led to a dramatic shift from prioritizing spectral efficiency towards energy efficiency [1], [2]. Furthermore, with the recent advancement in technological development, both energy and spectral efficiency are improving [2]. Moreover, multifold improvements are enabled by the introduction of holographic multi-input multi-output (MIMO) technologies. A holographic antenna is a two-dimensional (2D) antenna composed of numerous micro-antennas fabricated on a planar surface [3], [4]. These planar antennas also offer significant beamforming gains [5], resulting from their widened electromagnetic aperture with an almost infinite number of antenna elements. They are also classified into active and passive types, where one amplifies the incident signal while

the other does not. Advocating the immense advantages of holographic surfaces, their impact on reconfigurable reflecting surfaces (RIS) is an interesting area of research that is still unexplored to a larger extent. This is because the holographic RIS (HRIS) is conservative on power consumption while the traditional RIS employs many high-resolution phase shifters [6], demanding more power and making them less energy efficient. The reduction in power consumption was achieved by incorporating metamaterials and subwavelength-sized antennas, which imitated a continuous aperture [7]. The dense arrangement also enables the control of the electromagnetic (EM) environment with deterministic ability envisaged through channel hardening [8].

Note that the above-discussed articles presented their studies under the consideration of far-field assumptions. However, RIS is a technological advancement that has a wide spread of applications in wireless networks, such as in millimeter (mm)-wave frequencies where they exhibit a large aperture [9]. The consequence of this large aperture is the extension of the range of near-field region by many-folds, and notably, far-field assumptions may not be suitable. A prominent characteristic of the near-field region is the dominance of the distance-aware spherical wavefront, which allows beamfocusing to deliver wireless energy to a spatial location configured with three-dimensional spherical polar co-ordinate [10]. Compared to far-field communication, near-field communication provides higher spectral efficiency and a higher spatial degree of freedom. Further, depending on the distance (Rayleigh distance), deploying an RIS to provide wireless services within a nearby region is likely to cause communication to occur in the near field. For example, the feasibility of RIS-aided near-field communication was verified in [11], where closed-form expressions for near-field and far-field boundaries were derived. In [12], a RIS-aided near-field communication scenario was investigated, where the sum-rate maximization problem was addressed using the alternating optimization (AO) algorithm. Nonetheless, mmWave suffers from rapid outages and shadowing, which limits its operation range. To mitigate this problem and achieve extended range, HRIS is a promising technology [13], [14]. Additionally, HARIS is a prominent solution to reduce the

Additionally, $\Phi = \text{diag}(\Phi_1, \dots, \Phi_M) \in \mathbb{C}^{M \times M}$ represents the beamforming/phase shift matrix at the HARIS, where each element is defined as $\phi_m = \alpha_m e^{j\beta_m}$. Here, $\alpha_m = |\Phi[m, m]|$ and $\beta_m = \arg(\Phi[m, m]) \in [0, 2\pi]$ denote the amplification factor and phase shift at the m^{th} reflecting element of the HARIS. The external noise generated by the HARIS during signal amplification is denoted by $\mathbf{n}_A \sim \mathcal{CN}(0, \sigma_A^2 \mathbf{I})$, and the additive white Gaussian noise (AWGN) at the Alice is represented by $\mathbf{n}_1 \sim \mathcal{CN}(0, \sigma_1^2 \mathbf{I})$. Note that each user transmits its respective symbol simultaneously, with $x_k = \sqrt{P_k} s_k, \forall k \in \mathcal{K}$, where s_k is the confidential information sent to the BS by each user, and P_k is the transmit power used by each user. The corresponding combined signal received at the BS is given by

$$\mathbf{y} = \sum_{k=1}^K \sqrt{P_k} \mathbf{G} \Phi \mathbf{g}_k(\mathbf{f}_k) x_k + \mathbf{G} \Phi \mathbf{n}_A + \mathbf{n}_1, \quad (3)$$

Note that, using (3), BS decodes the symbol of each using the combining vector of the respective user, which is given by

$$\begin{aligned} y_k &= \mathbf{v}_k^H \mathbf{G} \Phi \mathbf{g}_k(\mathbf{f}_k) x_k + \sum_{i \neq k, i=1}^K \mathbf{v}_k^H \mathbf{G} \Phi \mathbf{g}_i(\mathbf{f}_i) x_i \\ &\quad + \mathbf{v}_k^H \mathbf{G} \Phi \mathbf{n}_A + \mathbf{v}_k^H \mathbf{n}_1. \end{aligned} \quad (4)$$

where $\mathbf{v}_k^H \in \mathbb{C}^{N \times 1}$ represent the combining vector corresponding to U_k . The signal-to-interference-plus-noise-ratio (SINR) corresponding to (4) is obtained as

$$\Upsilon_k^A = \frac{P_k |\mathbf{v}_k^H (\mathbf{G} \Phi \mathbf{g}_k(\mathbf{f}_k))|^2}{\Lambda_k + \|\mathbf{v}_k^H \mathbf{G} \Phi\|^2 \sigma_A^2 + \|\mathbf{v}_k\|^2 \sigma_1^2}, \quad (5)$$

where $\Lambda_k = \sum_{i \neq k, i=1}^K P_i |\mathbf{v}_k^H (\mathbf{G} \Phi \mathbf{g}_i(\mathbf{f}_i))|^2$. Using (5), the rate for the U_k is written as

$$R_k = \log_2(1 + \Upsilon_k^A). \quad (6)$$

III. PROBLEM FORMULATION AND PROPOSED SOLUTION

In this paper, we aim to maximize the sum-rate at the BS while ensuring a minimum QoS performance for each user within the available resource constraints. For the same, we formulate a sum-rate maximization problem as follows

$$\mathcal{P}_0 \quad \max_{\mathcal{P}, \mathbf{V}, \Phi} \sum_{k=1}^K R_k \quad (7a)$$

$$\text{s.t.} \quad \sum_{k=1}^K P_k \|\Phi \mathbf{g}_k(\mathbf{f}_k)\|^2 + \|\Phi\|_F^2 \sigma_A^2 \leq P_A, \quad (7b)$$

$$P_k \leq P_{max}, \forall k \in \mathcal{K}, \quad (7c)$$

$$R_k \geq R_{k, min}, \forall k \in \mathcal{K}, \quad (7d)$$

$$\alpha_m \leq \alpha_{m, max}, m = \{1, 2, \dots, M\}, \quad (7e)$$

$$\|\mathbf{v}_k\| = 1, \forall k \in \mathcal{K}, \quad (7f)$$

where $\mathcal{P} = [P_1, \dots, P_k, \dots, P_K]$ and $\mathbf{V} \triangleq [\mathbf{v}_1, \dots, \mathbf{v}_k, \dots, \mathbf{v}_K]$. Note that (7b) represents the maximum amplification allowed at the active RIS, (7c) corresponds to the maximum transmit power available at each user, and constraint (7d) ensures a minimum rate of $R_{k, min}$ at each user. In (7e), $\alpha_{m, max}$ represents the maximum amplification coefficient for the m -th reflecting element, while (7f) corresponds to the unit energy constraint related to the decoding vector for each user. As observed in constraints (7a), (7b), and (7d), the problem

\mathcal{P}_0 is inherently non-convex due to the coupling of variables. Therefore, we apply the AO technique to find the optimal values for \mathcal{P} , \mathbf{V} , and Φ .

Note that, for given \mathcal{P} and Φ , it is well-established that the linear MMSE equalizer is the optimal receive beamformer for maximizing the SINR of each U_k [23]. Thus, the MMSE-based equalizer for U_k can be formulated as

$$\mathbf{v}_k^* = \frac{\left(\sum_{i=k}^K \mathbf{t}_i \mathbf{t}_i^H P_i + \sigma_A^2 \mathbf{G} \Phi \Phi^H \mathbf{G}^H + \sigma_1^2 \mathbf{I}_N \right)^{-1} \mathbf{t}_k \sqrt{P_k}}{\left\| \left(\sum_{i=k}^K \mathbf{t}_i \mathbf{t}_i^H P_i + \sigma_A^2 \mathbf{G} \Phi \Phi^H \mathbf{G}^H + \sigma_1^2 \mathbf{I}_N \right)^{-1} \mathbf{t}_k \sqrt{P_k} \right\|}, \quad (8)$$

where $\mathbf{t}_i = \mathbf{G} \Phi \mathbf{g}_i$. After obtaining $\{\mathbf{v}_k^*\}$, we further simplify the problem by adopting the auxiliary variable $\zeta = [\zeta_1, \dots, \zeta_k, \dots, \zeta_K]$ and using (8). The simplified problem is given by

$$\mathcal{P}_1 \quad \max_{\mathcal{P}, \Phi, \zeta} \sum_{k=1}^K \zeta_k \quad (9a)$$

$$\text{s.t.} \quad R_k \geq \zeta_k, \forall k \in \mathcal{K}, \quad (9b)$$

$$\zeta_k \geq R_{k, min}, \forall k \in \mathcal{K}, \quad (9c)$$

$$(7b), (7c), (7e),$$

The Problem \mathcal{P}_1 is non-convex following the convex-concave nature of the objective function in (9a). In order to overcome this, we use the epigraph form to reformulate the problem \mathcal{P}_1 as follows:

$$\mathcal{P}_2 \quad \max_{\mathcal{P}, \Phi, \zeta} \sum_{k=1}^K \zeta_k \quad (10a)$$

$$\text{s.t.} \quad \frac{P_k |\mathbf{v}_k^H (\mathbf{G} \Phi \mathbf{g}_k(\mathbf{f}_k))|^2}{\Lambda_k + \|\mathbf{v}_k^H \mathbf{G} \Phi\|^2 \sigma_A^2 + \|\mathbf{v}_k\|^2 \sigma_1^2} \geq 2^{\zeta_k} - 1, \forall k \in \mathcal{K}, \quad (10b)$$

$$(7b), (7c), (7e), (9c).$$

Furthermore, we employ the AO method to address the non-convexity emerging from the coupling of variables \mathcal{P} and Φ . In particular, \mathcal{P} and Φ are alternately optimized in an iterative process, where each variable is updated sequentially. The specifics of this approach are detailed in the following sub-sections.

A. Sub-Optimum Power Allocation

Given Φ , problem \mathcal{P}_0 can be reformulated to find the sub-optimum \mathcal{P} as follows

$$\mathcal{P}_3 \quad \max_{\mathcal{P}, \zeta, F} \sum_{k=1}^K \zeta_k \quad (11a)$$

$$\text{s.t.} \quad P_k |\mathbf{v}_k^H (\mathbf{G} \Phi \mathbf{g}_k(\mathbf{f}_k))|^2 \geq (2^{\zeta_k} - 1) F_k, \forall k \in \mathcal{K}, \quad (11b)$$

$$\begin{aligned} &\sum_{i=1, i \neq k}^K P_i |\mathbf{v}_k^H (\mathbf{G} \Phi \mathbf{g}_i(\mathbf{f}_i))|^2 + \|\mathbf{v}_k^H \mathbf{G} \Phi\|^2 \sigma_A^2 \\ &+ \|\mathbf{v}_k\|^2 \sigma_1^2 \leq F_k, \forall k \in \mathcal{K}, \end{aligned} \quad (11c)$$

$$(7c), (9c),$$

where $F = [F_1, \dots, F_k, \dots, F_K]$ is the auxiliary variable. Note that using the Taylor's approximation at $\zeta_k^{(n)}$ and $F_k^{(n)}$, the problem \mathcal{P}_3 can be simplified as

$$\mathcal{P}_4 \quad \max_{\mathcal{P}, \zeta, F} \sum_{k=1}^K \zeta_k \quad (12a)$$

$$\begin{aligned} \text{s.t. } P_k |\mathbf{v}_k^H (\mathbf{G}\Phi \mathbf{g}_k(\mathbf{f}_k))|^2 &\geq (2^{\zeta_k^{(n)}} - 1)F_k \\ &+ 2^{\zeta_k^{(n)}} F_k^{(n)} (\zeta_k - \zeta_k^{(n)}), \forall k \in \mathcal{K}, \end{aligned} \quad (12b)$$

(7c), (9c), (11c).

The transformed problem \mathcal{P}_4 is converted into a standard convex problem [24] and is solved using CVX.

B. Design HARIS Beamforming

In this subsection, we design the optimal HARIS beamformer Φ for the obtained \mathcal{P} . The corresponding optimization problem is formulated as

$$\mathcal{P}_5 \quad \max_{\Phi, \tilde{\zeta}, \tilde{F}} \sum_{k=1}^K \tilde{\zeta}_k \quad (13a)$$

$$\text{s.t. } P_k |\mathbf{v}_k^H (\mathbf{G}\Phi \mathbf{g}_k(\mathbf{f}_k))|^2 \geq (2^{\tilde{\zeta}_k} - 1)\tilde{F}_k, \forall k \in \mathcal{K}, \quad (13b)$$

$$\begin{aligned} &\sum_{i=1, i \neq k}^K P_i |\mathbf{v}_k^H (\mathbf{G}\Phi \mathbf{g}_i(\mathbf{f}_i))|^2 + \|\mathbf{v}_k^H \mathbf{G}\Phi\|^2 \sigma_A^2 \\ &+ \|\mathbf{v}_k\|^2 \sigma_1^2 \leq \tilde{F}_k, \forall k \in \mathcal{K}, \end{aligned} \quad (13c)$$

(7b), (7e), (9c),

where $\tilde{\zeta} = [\tilde{\zeta}_1, \dots, \tilde{\zeta}_k, \dots, \tilde{\zeta}_K]$ and $\tilde{F} = [\tilde{F}_1, \dots, \tilde{F}_k, \dots, \tilde{F}_K]$ are the auxiliary variable. Similar to problem \mathcal{P}_3 , the problem \mathcal{P}_5 can also be solved using SDR transformation. The problem \mathcal{P}_5 is transformed to

$$\mathcal{P}_6 \quad \max_{\mathbf{Q}, \tilde{\zeta}, \tilde{F}} \sum_{k=1}^K \tilde{\zeta}_k \quad (14a)$$

$$\text{s.t. } \text{Tr}((\mathbf{H}_k) \mathbf{Q}) P_k \geq (2^{\tilde{\zeta}_k^{(n)}} - 1)\tilde{F}_k \\ + 2^{\tilde{\zeta}_k^{(n)}} \tilde{F}_k^{(n)} (\tilde{\zeta}_k - \tilde{\zeta}_k^{(n)}), \forall k \in \mathcal{K}, \quad (14b)$$

$$\sum_{i=1, i \neq k}^K \mathcal{Z}_i^A + \text{Tr}(\mathbf{H}_k^A \mathbf{Q}) \sigma_A^2 + \|\mathbf{v}_k\|^2 \sigma_1^2 \leq \tilde{F}_k, \quad (14c)$$

$$\text{Tr}((\mathbf{H}_A + \sigma_A^2 \mathbf{I}) \mathbf{Q}) \leq P_A \quad (14d)$$

$$\text{Tr}(\mathbf{L}_{M,r} \mathbf{Q}) \leq \alpha_r^2, \forall r \in \mathcal{M}, \quad (14e)$$

(9c),

where $\mathbf{Q} = \mathbf{q}\mathbf{q}^H$ with $\mathbf{q}^H = [\Phi_1, \dots, \Phi_m, \dots, \Phi_M]$ and $\mathbf{L}_{M,r}$ is a $M \times M$ matrix having r^{th} row and r^{th} column element as unity and other elements as zero. Here, the other terms in the problem \mathcal{P}_6 are defined as

$$\mathbf{H}_k = \text{diag}(\mathbf{v}_k^H \mathbf{G}) \mathbf{g}_k(\mathbf{f}_k) \mathbf{g}_k(\mathbf{f}_k)^H \text{diag}(\mathbf{v}_k^H \mathbf{G})^H, \quad (15)$$

$$\mathbf{H}_k^A = \text{diag}(\mathbf{v}_k^H \mathbf{G}) \text{diag}(\mathbf{v}_k^H \mathbf{G})^H, \quad (16)$$

$$\mathbf{H}_A = \sum_{k=1}^K P_k \text{diag}(\mathbf{g}_k(\mathbf{f}_k)) \text{diag}(\mathbf{g}_k(\mathbf{f}_k))^H, \quad (17)$$

$$\mathcal{Z}_i^A = \sum_{i=1, i \neq k}^K P_i \text{diag}(\mathbf{v}_k^H \mathbf{G}) \mathbf{g}_i(\mathbf{f}_i) \mathbf{g}_i(\mathbf{f}_i)^H \text{diag}(\mathbf{v}_k^H \mathbf{G})^H. \quad (18)$$

It is important to note that the constraints in problem \mathcal{P}_6 are convex, and both the numerator and denominator of the objective function exhibit linear dependence on the matrix \mathbf{Q} . Based on these observations, we propose an AO-based algorithm, **Algorithm 1**, to address problem \mathcal{P}_0 and find the optimal values for \mathcal{P} and Φ . In each iteration, \mathbf{v}_k is initially

Algorithm 1 Proposed Algorithm for Joint Optimization

1: Initialize $n = 0$, $\mathcal{P}^{(0)}$, $\mathbf{v}_k^{(0)}$, $\Phi^{(0)}$

Repeat:

2: Calculate $\mathbf{v}_k^{(n+1)}$ using (8).

3: Optimize $\mathcal{P}^{(n+1)}$ given $\Phi^{(n)}$ by solving \mathcal{P}_4 using CVX

4: Optimize $\Phi^{(n+1)}$ given $\mathcal{P}^{(n+1)}$ by solving \mathcal{P}_6 using CVX

5: $n = n + 1$,

Until: Convergence

6: Output $(\mathcal{P}^*, \mathbf{v}_k^*, \Phi^*)$

computed using (8) (as detailed in step 3), followed by solving problems \mathcal{P}_4 and \mathcal{P}_6 with CVX to determine \mathcal{P} (step 4) and Φ (step 5), respectively. This iterative procedure is repeated until convergence is achieved.

C. Computational Complexity

Let us consider that the solution for sub-optimum power allocation and HARIS beamforming in **Algorithm 1** converges within N_{\max}^{itr} iterations. The problems of sub-optimum power allocation in \mathcal{P}_4 has $3K + 1$ constraints and $NK + 4K$ variables, whereas the HARIS beamforming design in problem \mathcal{P}_6 has $3K + M$ constraints and $M + 4K$ variables. Hence, worst case complexity to obtain optimal \mathcal{P} and Φ can be given as $\mathcal{O}(N_{\max}^{\text{itr}}(3K + 1)^2(NK + 4K))$ and $\mathcal{O}(N_{\max}^{\text{itr}}(3K + M)^2(M + 4K))$, respectively. Thus, the overall computational complexity of the combined approach in **Algorithm 1** is given by

$$\mathcal{O}\left(N_{\max}^{\text{itr}} \left((3K + 1)^2(NK + 4K) + (3K + M)^2(M + 4K) \right)\right). \quad (19)$$

IV. SIMULATION RESULTS

In this section, several numerical examples have been carried out to exhibit the efficiency and convergence of the proposed algorithm through Monte Carlo simulations, averaging over 10^5 independent realizations of randomly generated channels. For the sake of simulation, The BS is located at (16.453m, 116.2630°, 72.0471°) while four users are located at (4.1472m, 78.3022°, 101.5349°), (8.6763m, 110.3402°, 79.7452°), and (14.6328m, 101.1328°, 119.5479°), respectively. The HARIS is located at the center of the coordinate (0, 0°, 0°). Further, unless otherwise specified, $\sigma^2 = \sigma_1^2 = \sigma_A^2 = -90\text{dBm}$, $K = 3$, $N = 12$, $P_k = 35\text{dBm}$, and $P_A = 10\text{dBm}$. Furthermore, the operating frequency is considered to 24GHz with a RIS aperture length of 1m. Therefore, the Fresnel and Rayleigh distance works out to be 1.3m and 160.2m, respectively. Therefore, any radio receiver lying within this range will experience the effect of near-field [21], [22], [25]. Hence, all the uplink users considered lie within the near-field region of the HARIS.

Fig. 2 illustrates the convergence characteristics of **Algorithm 1**, which is obtained with $P_{\max} = 35\text{ dBm}$, $P_A = 10\text{ dBm}$, $N = 12$, and $M(S \times T) = 256, 384, 512$. It can be observed that the algorithm converges after a few iterations,

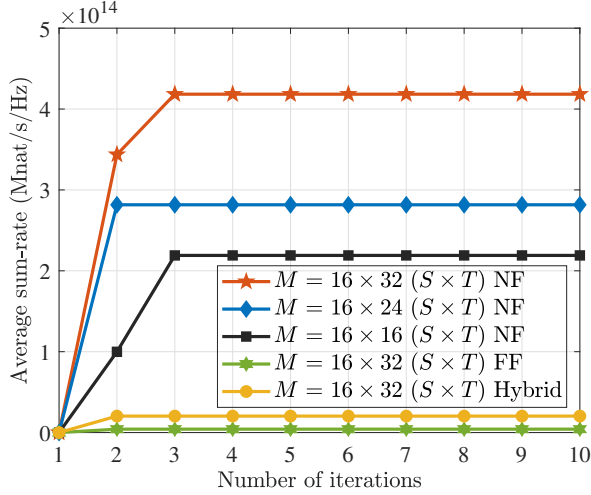


Fig. 2: Average sum-rate versus number of the iterations. ($K = 3, N = 12, P_{max} = 25\text{dBm}, P_A = 10\text{dBm}$).

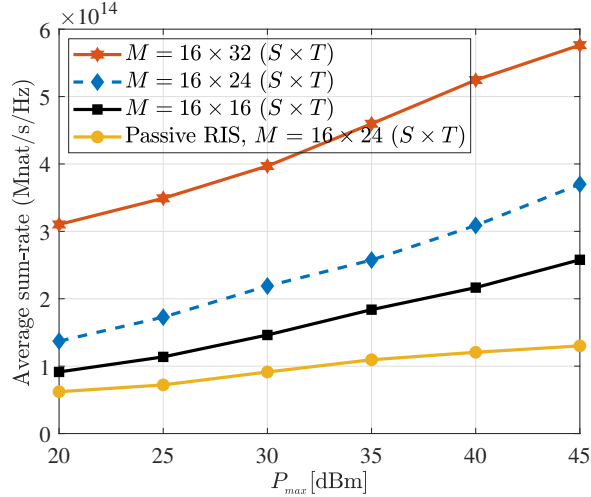


Fig. 3: Average sum-rate versus P_{max} for $K = 3, N = 12$, and $P_A = 10\text{dBm}$.

demonstrating its effectiveness. Furthermore, it can be seen that the average sum-rate improves as M increases due to the enhanced beamforming gain and amplified power, which substantially boosts the received signal strength. Moreover, we compared far-field and hybrid systems with higher values of M and we observed the near-field system provides better performance compared to far-field and hybrid systems.

Fig. 3 depicts the average sum-rate (in Mnat/s/Hz) versus the total transmit power P_{max} for different numbers of HARIS elements. It can be observed that the average sum-rate increases with an increase in P_{max} . The main reason for this is the increase in net SINR corresponding to each U_k at the BS due to the rise in the maximum available power for transmission at U_k . Furthermore, one can also observe that the joint amplification and reflection of the incident signal by the active RIS provide better performance compared to the passive RIS. However, this performance enhancement comes with an additional power consumption by the active RIS compared to the passive counterpart. Therefore, to use the full potential of

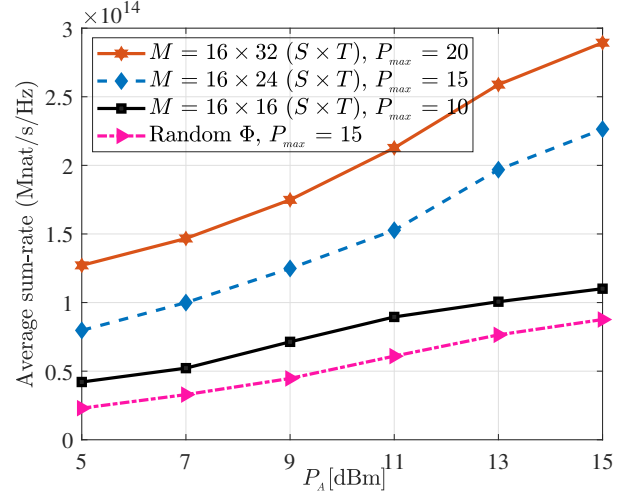


Fig. 4: Average sum-rate versus P_A . ($K = 3, N = 12$).

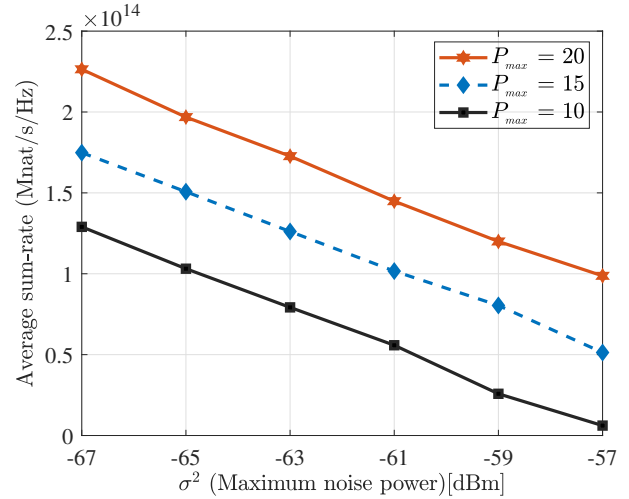


Fig. 5: Average sum-rate versus σ^2 ($K = 3, N = 12, P_A = 10\text{dBm}$).

active RIS, finding the optimum value of key metrics like \mathcal{P} and Φ using the proposed algorithm is significant.

Fig. 4 shows the average sum-rate against P_A for different values of M and P_{max} . It can be seen that, as P_A increases, more reflecting power becomes available for signal amplification, which causes the performance to increase as well. The main reason for this behavior is the fact that along with the signal amplification, the increasing P_A also increases the net power of the amplified noise. This forces the change in SINR to be negligible with increasing P_A . In addition, we also show the importance of the optimal solution provided by the proposed algorithm by comparing it with that of the random phase shift matrix with P_{max} . It can be seen that the solution provided by the proposed algorithm provides a significantly higher sum-rate compared to the random case.

Fig. 5 illustrates the average sum-rate versus maximum noise power (σ^2) for different values of P_{max} . It is observed that the average sum-rate decreases with an increase in σ^2 . This is due to the fact that the increase in noise power reduces the SINR, leading to a significant reduction in the achievable

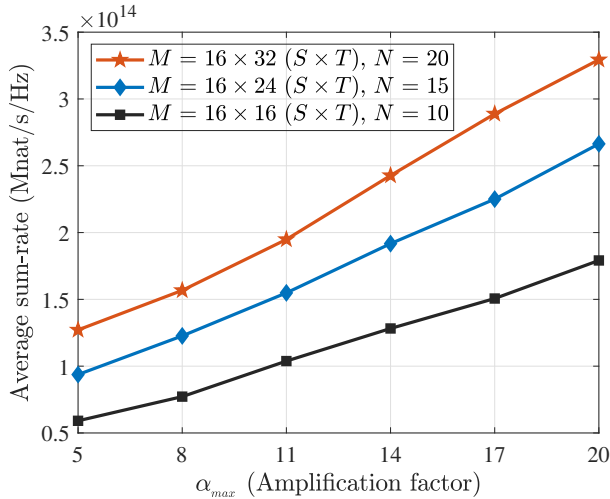


Fig. 6: Average sum-rate versus α_{max} . ($K = 3, P_{max} = 25\text{dBm}, P_A = 10\text{dBm}$).

rate. Additionally, we compared active RIS with passive RIS in terms of high noise power. Clearly, the use of HARIS provides an edge over passive HRIS to tackle unavoidable higher noise.

Fig. 6 depicts the average sum-rate versus α_{max} for various N values. It can be observed that the average sum-rate increases with an increase in α_{max} . This is due to the fact that a sufficient power budget is helpful in improving the net SINR corresponding to each user U_k at the BS due to the rise in the α_{max} .

V. CONCLUSION

In this work, we investigated the performance of a HARIS-based wireless network for near-field uplink communications. Further, in order to maximize the system performance, an AO-based algorithm was proposed to jointly optimize the power allocated to uplink users and the HARIS phase profile. The optimal power allocation value was obtained through convex upper bound approximation, while SDR programming was used to attain an optimal HARIS phase profile. Besides, several numerical simulations were performed to validate the efficacy and superiority of the proposed algorithm. The fast convergence of the algorithm, despite the variation in the number of elements, ensures the efficacy of the proposed algorithm. Furthermore, it is also observed that increasing the number of elements or power at the HARIS results in better system performance. However, an opposite trend is observed with the increase in noise power. As a consequence, it can be inferred that by properly tuning the active RIS amplification coefficient and the phase shift, it is possible to optimize the spectral efficiency of the network and mitigate unwanted power loss at the HARIS.

REFERENCES

[1] Z. Liwen, F. Qamar, M. Liaqat, M. N. Hindia, and K. A. Z. Ariffin, "Towards Efficient 6G IoT Networks: A Perspective on Resource Optimization Strategies, Challenges, and Future Directions," *IEEE Access*, May 2024.

[2] P. Yang, Y. Xiao, M. Xiao, and S. Li, "6G wireless communications: Vision and potential techniques," *IEEE Netw.*, vol. 33, no. 4, pp. 70–75, 2019.

[3] A. Pizzo, T. L. Marzetta, and L. Sanguinetti, "Spatially-stationary model for holographic MIMO small-scale fading," *IEEE J. Sel. Areas Commun.*, vol. 38, no. 9, pp. 1964–1979, 2020.

[4] C. Huang, S. Hu, G. C. Alexandropoulos, A. Zappone, C. Yuen, R. Zhang, M. D. Renzo, and M. Debbah, "Holographic MIMO surfaces for 6G wireless networks: Opportunities, challenges, and trends," *IEEE Wireless Commun.*, vol. 27, no. 5, pp. 118–125, 2020.

[5] S. Zeng, H. Zhang, B. Di, H. Qin, X. Su, and L. Song, "Reconfigurable refractive surfaces: An energy-efficient way to holographic MIMO," *IEEE Commun. Lett.*, vol. 26, no. 10, pp. 2490–2494, 2022.

[6] L. Dai *et al.*, "Reconfigurable intelligent surface-based wireless communications: Antenna design, prototyping, and experimental results," *IEEE Access*, vol. 8, pp. 45 913–45 923, 2020.

[7] C. Huang, S. Hu, G. C. Alexandropoulos, A. Zappone, C. Yuen, R. Zhang, M. Di Renzo, and M. Debbah, "Holographic MIMO surfaces for 6G wireless networks: Opportunities, challenges, and trends," *IEEE wireless commun.*, vol. 27, no. 5, pp. 118–125, 2020.

[8] C. You, Y. Cai, Y. Liu, M. Di Renzo, T. M. Duman, A. Yener, and A. L. Swindlehurst, "Next generation advanced transceiver technologies for 6G," 2024. [Online]. Available: <https://arxiv.org/abs/2403.16458>

[9] J. Xu, L. You, G. C. Alexandropoulos, X. Yi, W. Wang, and X. Gao, "Near-field wideband extremely large-scale MIMO transmissions with holographic metasurface-based antenna arrays," *IEEE Trans. Wireless Commun.*, 2024.

[10] H. Zhang *et al.*, "6G wireless communications: From far-field beam steering to near-field beam focusing," *IEEE Commun. Mag.*, vol. 61, no. 4, pp. 72–77, Mar. 2023.

[11] W. Chen *et al.*, "Beamforming design for RIS-aided mimo communication: A piece-wise near-field model," in *Proc. IEEE ICC Workshops*, Aug 2024, pp. 385–390.

[12] S. Lv, Y. Liu, X. Xu, A. Nallanathan, and A. L. Swindlehurst, "RIS-aided near-field MIMO communications: Codebook and beam training design," *IEEE Trans. Wireless Commun.*, vol. 23, no. 9, pp. 12 531–12 546, Sep. 2024.

[13] J. Tian, Y. Han, S. Jin, X. Li, J. Zhang, and M. Matthaiou, "Near-field channel reconstruction in sensing RIS-assisted wireless communication systems," *IEEE Trans. Wireless Commun.*, pp. 1–1, 2024.

[14] W. Chen, Z. Yang, Z. Wei, D. W. K. Ng, and M. Matthaiou, "RIS-aided MIMO beamforming: Piece-wise near-field channel model," 2024. [Online]. Available: <https://arxiv.org/abs/2406.14939>

[15] Z. Zhang, L. Dai, X. Chen, C. Liu, F. Yang, R. Schober, and H. V. Poor, "Active RIS vs. passive RIS: Which will prevail in 6G?" *IEEE Trans. Commun.*, vol. 71, no. 3, pp. 1707–1725, Mar. 2023.

[16] K. Zhi, C. Pan, H. Ren, K. K. Chai, and M. Elkashlan, "Active RIS versus passive RIS: Which is superior with the same power budget?" *IEEE Commun. Lett.*, vol. 26, no. 5, pp. 1150–1154, May 2022.

[17] R. Long, Y.-C. Liang, Y. Pei, and E. G. Larsson, "Active reconfigurable intelligent surface-aided wireless communications," *IEEE Trans. Wireless Commun.*, vol. 20, no. 8, pp. 4962–4975, Aug. 2021.

[18] C. You and R. Zhang, "Wireless communication aided by intelligent reflecting surface: Active or passive?" *IEEE Trans. Wireless Commun.*, vol. 10, no. 12, pp. 2659–2663, Dec. 2021.

[19] D. Xu, X. Yu, D. W. Kwan Ng, and R. Schober, "Resource allocation for active IRS-assisted multiuser communication systems," in *Proc. Asilomar Conf. Signals Syst. Computers*, Oct 2021, pp. 113–119.

[20] S. Singh, A. Raviteja, K. Singh, S. K. Singh, A. Kaushik, and M.-L. Ku, "Secrecy rate maximization for active RIS-aided robust uplink NOMA communications," *IEEE Wireless Commun. Lett.*, pp. 1–1, 2024.

[21] Y. Liu, Z. Wang, J. Xu, C. Ouyang, X. Mu, and R. Schober, "Near-field communications: A tutorial review," *IEEE Open J. Commun. Soc.*, vol. 4, pp. 1999–2049, 2023.

[22] N. Song and H. Dai, "Optimal beam-focusing design for 6g near-field swipt systems," *IEICE Commun. Exp.*, vol. 13, no. 3, pp. 84–87, 2024.

[23] X. Yang, H. Wang, and Y. Feng, "Sum rate maximization for active RIS-aided uplink multi-antenna NOMA systems," *IEEE Trans. Wireless Commun.*, vol. 12, no. 7, pp. 1149–1153, 2023.

[24] S. Boyd and L. Vandenberghe, *Convex optimization*. Cambridge university press, 2004.

[25] Z. Wang, X. Mu, and Y. Liu, "Near-field integrated sensing and communications," *IEEE Commun. Lett.*, vol. 27, no. 8, pp. 2048–2052, 2023.